Design and Capabilities of NIST's Scale-Model Smokestack Simulator (SMSS)

Aaron N. Johnson[1], Joey T. Boyd[1], Eric Harman[2], Mark Khalil[1], Jacob R. Ricker[1],
Chris J. Crowley[1,] John D. Wright[1], Rodney A. Bryant[1], and Iosif Shinder[1]

National Institute of Standards and Technology (NIST)[1]
Colorado Engineering Experimental Station Inc. (CEESI)[2]
Corresponding Author: Aaron.Johnson@nist.gov, 301-975-5954

Abstract

The amount of CO_2 emitted from a coal-fired power plant (CFPP) is measured by continuous emissions monitoring systems (CEMS) permanently installed in the exhaust smokestack. Both the CO_2 concentration and the bulk flow are continuously measured by CEMS, and the product of these measurements gives the CO_2 flux. The EPA requires CEMS to be calibrated yearly using a test procedure called a relative accuracy test audit (RATA). This calibration procedure links the concentration measurement to the SI through reference gas standards. However, establishing flow traceability is more difficult because the CEMS flow meter and the flow meter used to perform the RATA can be adversely affected by the complex velocity fields (i.e., swirling flow with a skewed velocity profile) prevalent in smokestacks. As a result the RATA only provides "relative accuracy" instead of flow traceability to a primary standard. In order to quantify the uncertainty of smokestack flow measurements, and to establish a calibration platform with documented traceability to the derived SI unit of flow, NIST constructed a $1/10^{th}$ scale model smokestack simulator (SMSS). The test section of the SMSS will have the same velocity range and similar flow distortions found in to a typical CFPP smokestack. However, the SMSS will provide reference flow measurements at expanded uncertainties of less than 1 %. This manuscript discusses the design and capabilities of the SMSS and presents Computational Fluid Dynamics (CFD) results of the expected velocity field in the SMSS facility.

1. INTRODUCTION

Coal-fired power plants (CFPPs) are the world's largest producer of electric energy; however, they are also a significant source of the greenhouse gas (GHG) carbon dioxide, as well as a wide variety of other air pollutants (*e.g.*, mercury, carbon monoxide, sulfur dioxide, nitrous oxides). Air pollutants emitted by CFPPs must be measured at sufficiently low uncertainties to ensure compliance with regulations and to assess ongoing GHG mitigation efforts. Currently, air pollutants are measured in the United States using continuous emissions monitoring systems (CEMS) installed in CFPP exhaust smokestacks.

Continuous emissions monitoring systems consist of instrumentation to measure both the concentration of regulated pollutants and the bulk mass flow in the smokestack. These measurements are made near the top of the smokestack, which can be 100 m or more above the ground. The product of pollutant concentration and the bulk mass flow is the emission rate of a given pollutant. The emission rate is reported to the EPA[1] for each pollutant, and the EPA calculates the total annual emission levels.

---

[1] The acronym EPA denotes the U.S. Environmental Protection Agency.

The EPA has historically used CEMS measurements to assess compliance of CFFPs with federal air emission standards. In 2014, the EPA announced its Clean Power Plan requiring CFPPs to reduce their CO_2 emissions by 30 % relative to 2005 levels [1]. The current uncertainty of CEMS measurements may be too large to equitably assess compliance of this new regulation. Large dispersions (of approximately 20 %) between CEMS CO_2 emissions measurements and EIA[2] mass balance calculations [2, 3], have prompted an international effort to assess the CEMS uncertainty. A first step toward this goal is to establish a chain of traceability linking CEMS measurements to national standards. Such a pathway exists for CEMS composition measurements, which are traceable to the SI[1] via calibrated reference gases [4]. In contrast, flow traceability has not been established due to the size and complexity of smokestack flows. No flow calibration laboratory has the capacity to accommodate the large sizes (*i.e.*, typical smokestack diameters range from 10 m to 15 m) or to calibrate the large flows (up to 5000 m^3/s) of CFPP smokestacks. In addition, the velocity field in smokestacks is complex, generally consisting of turbulent, asymmetric, swirling flow. These flow conditions can significantly degrade CEMS flow meter performance.
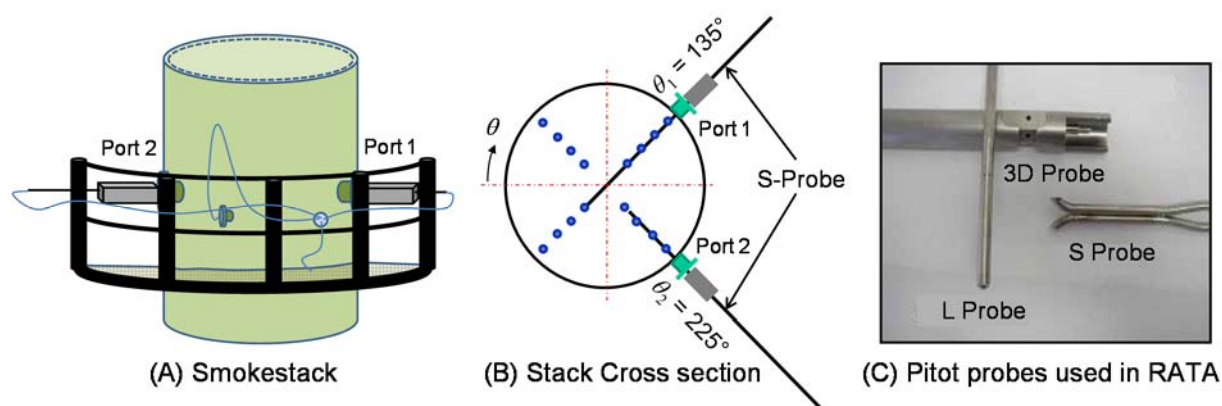

Figure 1. (A) Section of the smokestack showing 2 orthogonal ports used to insert pitot probes, (B) schematic of the points (●) along 2 diametric chords in the smokestack cross section and where velocities are measured during a pitot traverse, and (C) Various types of differential pressure probes that are used to measure the velocity.

The fidelity of CEMS flow and concentration measurements are currently assessed using an EPA testing protocol called a *relative accuracy test audit* (RATA). The flow component of the RATA uses a pitot probe traversing method to calibrate the CEMS flow monitor. A pitot probe is inserted into each of the ports shown in Fig. 1A, and traversed across the cross section of the smokestack along two orthogonal, diametric, chords. The pitot probes measure the velocity of the stack gas at the discrete points denoted by the solid circles (●) shown in Fig. 1B. The resulting pitot probe velocities are averaged and multiplied by the cross sectional area to determine volumetric flow. Measurements of the pressure, temperature, and molar mass are used to determine the flue gas density, which is multiplied by the calculated volumetric flow to determine the mass flow. The relative accuracy is the percent difference between the mass flow determined by the RATA and that based on the CEMS flow measurement.

Figure 1C shows three types of pitot probes including 1) a standard L-type pitot probe, 2) an S-type pitot probe, and 3) a three dimensional pitot probe. All of these probes have the same basic principle of operation. Differential pressure measurements across the appropriate ports of the pitot probes correlate (via calibration) to the fluid velocity. While any of these probes can be used for the RATA, the S probe is by far the most widely used; therefore the uncertainty characteristics of this probe are important to quantify [5, 6]. In 2012, Reader-Harris estimated that the measurement uncertainty of the S-type pitot traverse method (not including uncertainties from the CEMS flow meter) can be as large as 11.8 % [7].

The flow component of a RATA adheres to government protocols documented in EPA Methods 1 and 2 [8, 9, 10, 11, 12, 13]. These protocols have formed the basis of CEMS flow measurements for more than two decades. The RATA, however, does not determine the uncertainty of a CEMS measurement, but instead only provides *relative accuracy* or the percent difference between the EPA Method and the CEMS flow monitor. Even if this difference is small, it does not guarantee a low uncertainty flow measurement. Past researchers have found that the flow conditions (*i.e.,* turbulent, asymmetric, swirling flow) in smokestacks can adversely affect pitot probes used in the RATA flow measurement [14, 15]. A CEMS flow monitor that is recurrently calibrated against the same type of probe in the same flow conditions could agree with the biased RATA and yet have a significant uncertainty.

NIST's 1/10th scale model smokestack simulator (SMSS) was developed to independently determine the in-situ performance and uncertainty of smokestack flow measurement technologies. In particular, we will focus on 1) characterizing the S-Probe, which is widely used in the EPA RATA, and 2) evaluating the ultrasonic flow meter, which is widely used for CEMS flow measurements [16]. The SMSS is designed to simulate the asymmetric velocity profiles and swirling flows prevalent in CFPP smokestacks. However, in contrast to current smokestack flow measurements, the flow will be determined using a reference standard flow meter with well documented traceability to NIST primary flow measurement standards and with an expanded uncertainty of less than 1 %. In this manuscript we discuss the design and capabilities of the SMSS, and we present CFD results of the velocity field and pressure distribution.

2. CFPP SMOKESTACK FLOW MEASUREMENT CHALLENGES

Accurately measuring the flow in smokestacks is difficult because installation effects degrade the performance of the CEMS flow meter. Installation effects occur because the piping configuration used to direct the flow into the smokestack significantly distorts the velocity field (*e.g.*, flow separation, recirculation zones, asymmetric or skewed velocity profiles, and swirl). The piping network immediately upstream of smokestacks is often designed with curved pipes, reducers, fans, and sharp corners all of which cause installation effects. Figure 2A depicts a typical smokestack design where the flow is directed through a series of piping installations before reaching the smokestack. A qualitative sketch depicting the major features of the velocity field is shown in Fig. 2B. First, a recirculation zone forms in the cavity at the base of the smokestack. Low frequency oscillations in the recirculation zone can result in time-dependent velocity profiles that increase the uncertainty of flow measurements. Second, inertial forces divert streamlines preferentially toward the outer wall as flow passes through the sharp 90° elbow. The resulting velocity profile is asymmetric with the highest velocities occurring near the outer wall of the smokestack as shown

in Fig. 2B [17, 18]. Third, along the inner wall of the 90° elbow, the flow may separate and move in the opposite direction (*i.e.*, reverse flow). Fourth, a secondary swirling flow consisting of two counter-rotating vortices [19] is established in the cross sectional plane.[3] The secondary flow is caused by an imbalance between 1) inertial forces directing the fluid toward the outer wall and 2) a favorable pressure gradient directed toward the inner wall. Near the wall the velocity (retarded by the boundary layer) is lower and the favorable pressure gradient accelerates the fluid toward the inner wall. Near the axis, the velocity is larger and inertial effects dominate the pressure gradient accelerating the fluid toward the outer wall.
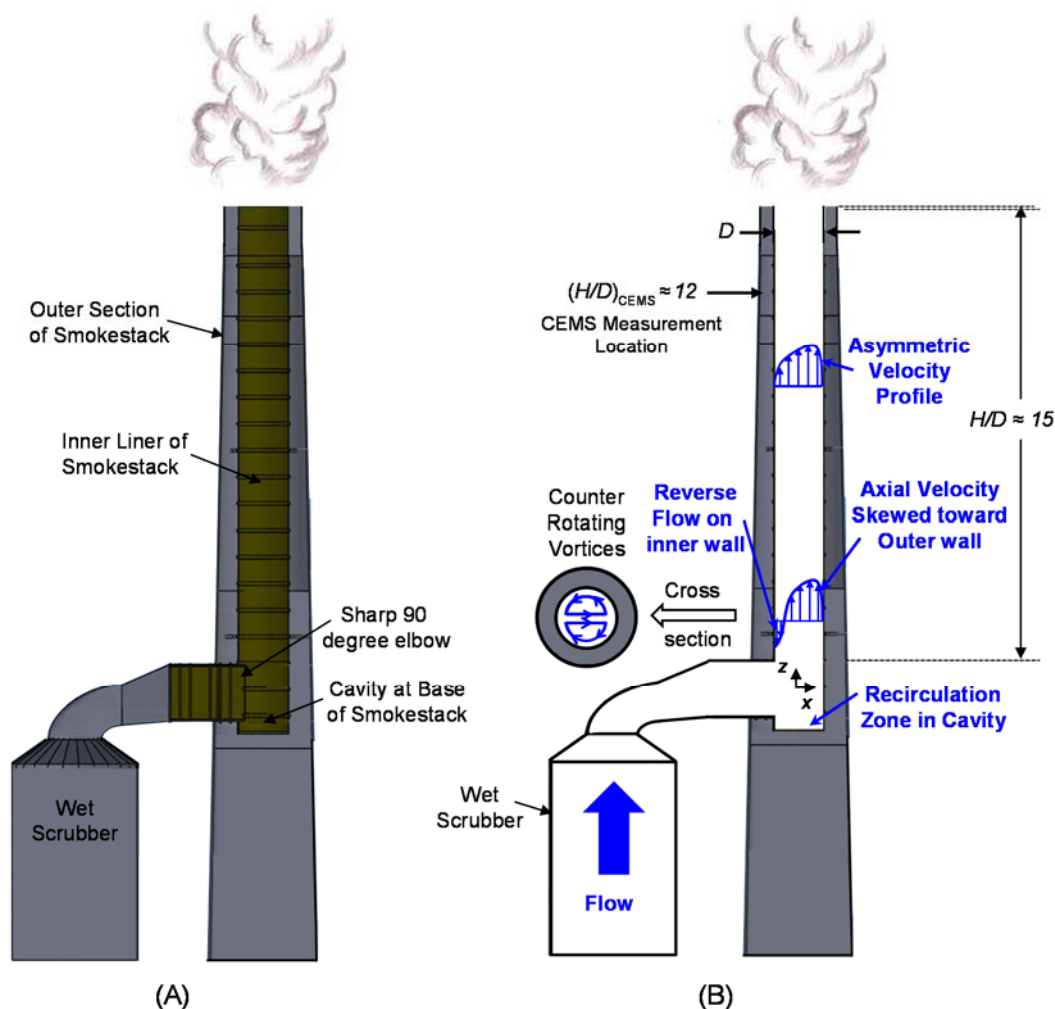

Figure 2. (A) Typical CFPP smokestack geometry, and (B) a qualitative sketch of velocity field. (Note: *H* is the height of the smokestack immediately after sharp 90° elbow and *D* is the smokestack internal diameter).

As the flow advances toward the top of the smokestack, the separated region reattaches so that the axial velocity is positive everywhere in the flow field (*i.e.*, no reverse flow). However, the flow distortions (*i.e.*, asymmetric velocity profile and swirl) persist to the CEMS measurement location. For reasons of structural integrity and cost, CFPP smokestacks are typically designed with height

---

[3]   Here we take the swirl to be caused solely by the sharp 90° elbow so that the secondary flow consists of two counter-rotating vortices. In practice, swirling flow patterns will differ depending on the configuration of the upstream piping system.

(H) to diameter (D) ratios of $H/D \leq 15$, and the CEMS measurements are often made at a height equal to 80 % of H or $(H/D)_{CEMS} < 12$. On the other hand, numerous experiments have shown that swirl, and velocity profile asymmetries can persist for distances greater than 100 D [19]. As a result CEMS flow measurements and the RATA are made in regions where installation effects are significant.

3. OVERVIEW OF THE SCALE MODEL SMOKESTACK SIMULATOR (SMSS) FACILITY

The SMSS shown in Fig. 3 is essentially a 1/10th scale horizontal smokestack that uses air as a surrogate for flue gas. To keep the cost reasonable and to facilitate convenient access to the test section, the SMSS was oriented horizontally rather than in the vertical configuration used in CFPP smokestacks. The difference in geometric orientation is only significant for CFPPs that exhaust hot flue gases. For these CFPPs, buoyancy driven flow will result in a different characteristic velocity field than the SMSS. However, most modern CFPPs are equipped with wet scrubbers to remove SO_2. As a result, the flue gas exhaust temperature is not substantially above the ambient temperature, and buoyancy effects are not significant relative to forced convection by blowers. Therefore, the velocity field distortions in typical CFPP smokestacks are closely approximated in the test section of the horizontal SMSS.
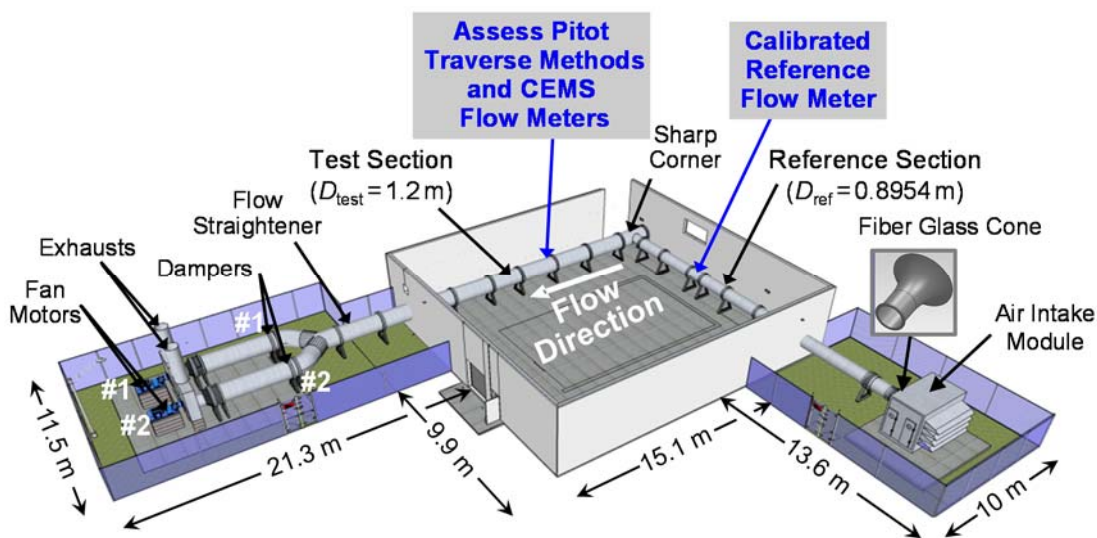

Figure 3. Schematic of the NIST's Scale Model Smokestack Simulator (SMSS).

We built the SMSS facility to accomplish 5 main goals:

1) to quantify the uncertainty of EPA RATA in distorted flows,

2) to characterize the performance and uncertainty of CEMS ultrasonic flow meters in the distorted smokestack flows (as a function of velocity, installation angle, swirl level, profile distortion, number of paths, path configuration, number of pipe diameters from installation effect),

3) to generate benchmark data to validate turbulent CFD models that will be used to scale-up NIST results to industrial size CFPP smokestacks,

4) to explore alternative methods of measuring flue gas flows, and

5) to provide a flow calibration rig for RATA companies to demonstrate their measurement capabilities and prove their uncertainty.

The operation of the SMSS can be separated into 3 stages that include; a) generating and maintaining a steady flow; b) measuring the flow at an expanded uncertainty of 0.5 % in the reference section; and c) establishing a known flow with a distorted velocity field in the test section.

3.1. Generating and Maintaining a Steady Flow

Ambient air is drawn into the intake module by the two fans at the facility exit as shown in Figs. 3, 4A, and 4C. The rotational speeds of the fans, and therefore the flow velocities in the test section, are controlled by two variable frequency drives (VFDs) located in the SMSS Building. Velocity readings from a flow meter installed in the reference section are converted to the test section velocity[4] to provide feedback to each VFD. The VFDs continually adjust the fan speed to achieve the desired set point velocity. The system is design to provide flow stabilities better than 0.5 % over the full operating range. The maximum velocity in the test section is 13 m/s using one fan and increases to 26 m/s when both fans are used together.
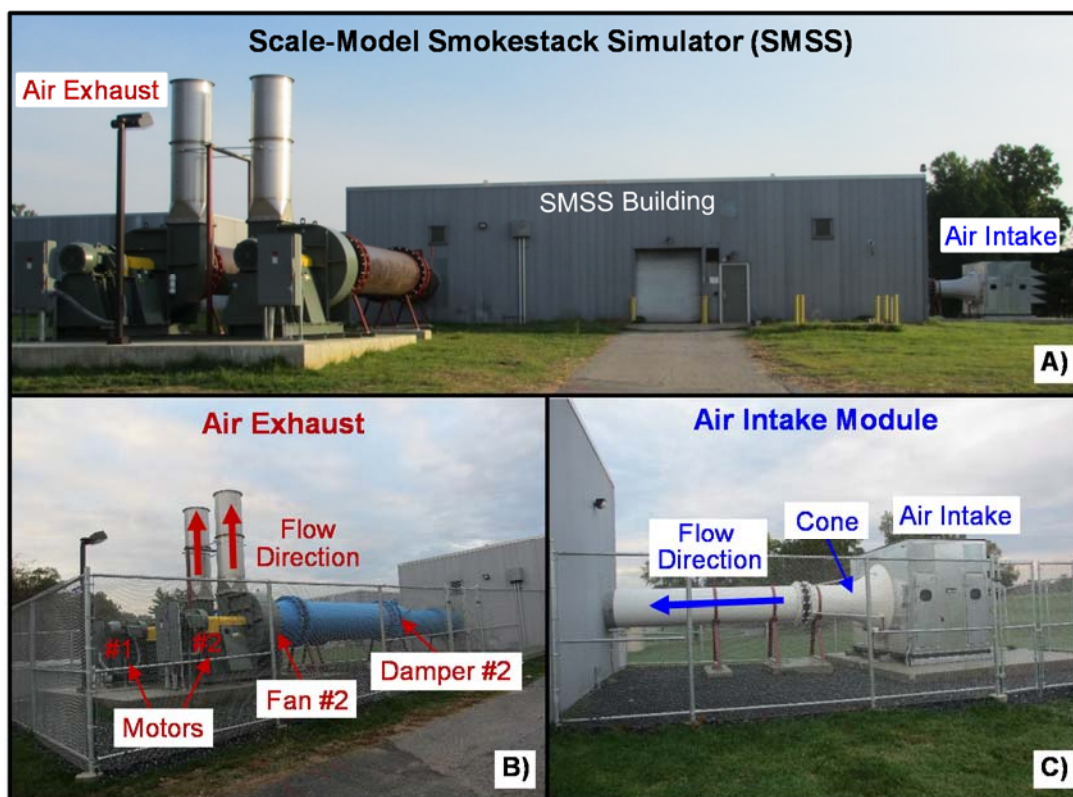

Figure 4. NIST Scale-Model Smokestack Simulator A) Front view, B) Air Exhaust, and C) Air Intake Model.

The SMSS is operated using custom software that controls the startup and shutdown of the facility. At startup the software opens the inlet damper shown in Fig. 5C. The software determines if both fans are needed to attain the desired set point velocity. If only one fan is necessary the operator can select which fan to use. Based on the fans selected, the appropriate fan motors are started and the VFD ramps the flow velocity to the desired set point. When the designated fan motor is

---

4   The velocity in the test section is calculated by multiplying the reference section velocity by the area ratio $(A_{\mathrm{ref}}/A_{\mathrm{test}})$ where A_{ref} and A_{test} are the cross sectional areas of the reference section piping and test section piping, respectively.

engaged, the corresponding spring-loaded damper (shown in Figs. 3 and 4B) opens to allow flow. At shutdown, the VFD ramps down the flow and then closes the inlet damper.
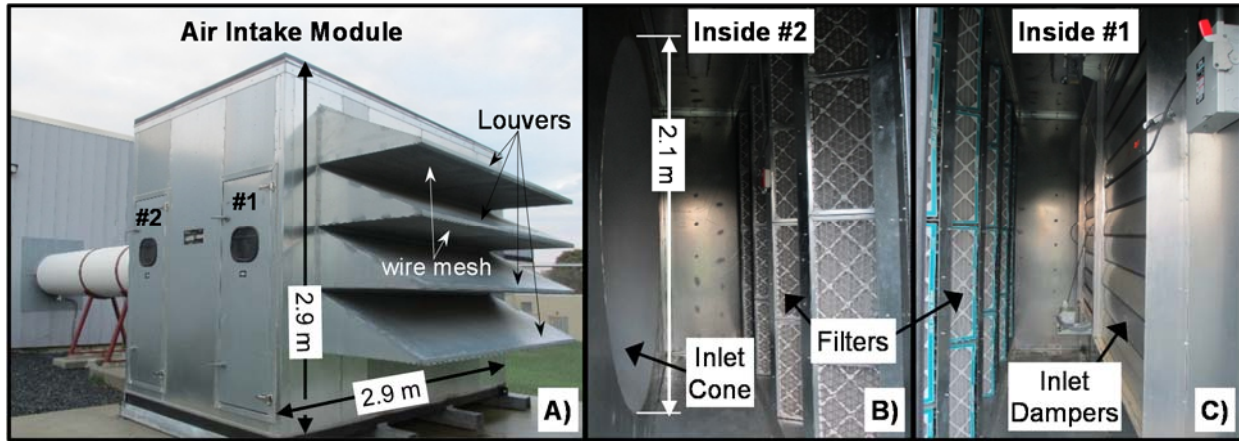

Figure 5. Air Intake Module A) Entry points #1 and #2, inlet louvers, and 1.27 cm wire mesh and, B) Filters and Inlet Cone, and C) Inlet Dampers and Filters.

3.2. NIST Traceable Flow Measurement in the Reference Section

The SMSS is designed to produce nearly ideal flow conditions (*i.e.*, a symmetric velocity profile with negligible swirl) in the reference section. The well-conditioned flow is measured using an 8 path ultrasonic flow meter (USM) with an expanded uncertainty of 0.5 % at a 95 % confidence level. Figure 6 shows the installation of the USM in the reference section. It is installed 13.2 D_{ref} downstream of the cone exit plane.
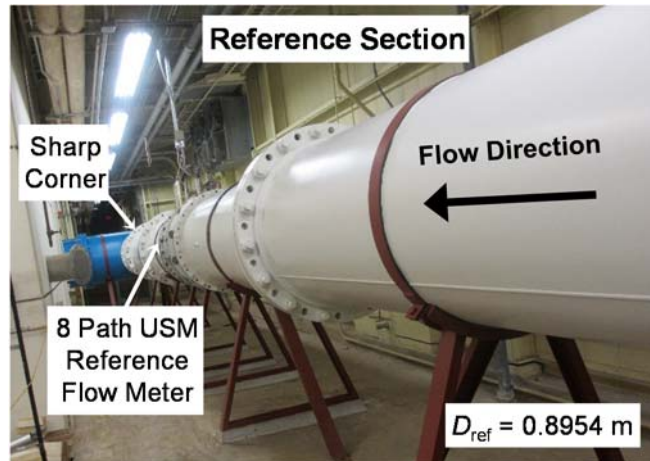

Figure 6. 8 path ultrasonic flow meter (USM) installed in reference section pipe.

Flow conditioning begins in the intake module shown in Fig. 5. First, the inlet louvers and 1.27 cm wire meshing in Fig. 5A prevent debris from entering into the flow stream as air is drawn into the intake module. The intake louvers are oriented downward to inhibit rain from being drawn into the facility. The smaller filters in Figs. 5B and 5C remove debris larger than 10 μm (*e.g.*, dust, rust, bugs). The air exiting the filter in Fig. 5B is directed into the fiber glass cone, which has a circular cross section with an inlet diameter of D_{inlet} = 2.1 m. The fiber glass cone converges to an exit diameter that matches the reference section piping (*i.e.*, D_{outlet} = 0.8954 m).

The cone functions as a flow conditioner by reducing asymmetries in the axial velocity profile. The flow acceleration through the constant curvature convergent section is designed to produce a nearly uniform velocity profile at the exit plane of the cone. The straight length of piping downstream of the cone and upstream of the USM provides additional flow conditioning to further develop the axial velocity profile and to attenuate transverse velocity components introduced at the inlet. Nevertheless, the USM (by virtue of its 8 path design) is highly immune to small levels of asymmetry and swirl. As such, we do not expect that installation effects will contribute to the uncertainty of the flow measurement in the reference section.

Computational Fluid Dynamics (CFD) Modeling of Reference Section Flow
During the design phase we computed the pressure and velocity field in the SMSS using the commercial CFD software ANSYS FLUENT.[5] We modeled the flow field using the 3D, steady, incompressible Reynolds Averaged Navier-Stokes (RANS) equations. The working fluid was taken to be air with a uniform density of ρ = 1.225 kg/m^3 and a uniform viscosity of μ = 1.79 × 10^{-5} kg/(m·s). The effects of turbulence were modeled using the realizable k-ε turbulence model with enhanced wall functions.
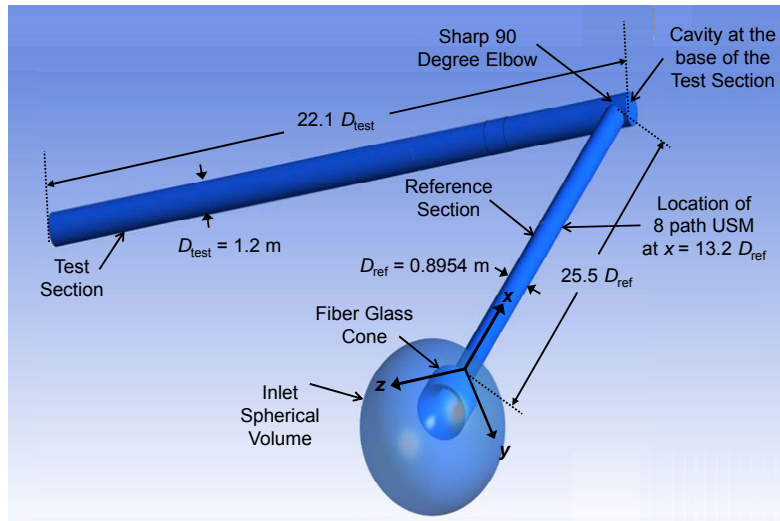

Figure 7. CFD Geometry of SMSS.

Figure 7 shows the numerical domain used to model the SMSS including an inlet spherical volume, fiber glass cone, reference section, sharp 90° elbow, and test section. The origin of the coordinate system is centered on the exit plane of the fiber glass bell so that the 25.5 D_{ref} diameters of straight pipe in the reference section begins at x = 0. The x-axis coincides with the axis of the reference section while the z-axis is parallel to the test section axis. Boundary conditions are specified at the exit of the test section, along the interior walls of the SMSS, and along the inlet spherical volume.[6] The flow enters perpendicularly into the spherical volume and the pressure along its surface is taken to be 101.325 kPa. No-slip conditions are enforced along pipe walls. At the exit plane we specify the pressure drop (ΔP) and extrapolate the velocity from upstream

---

[5]   In order to describe materials and procedures adequately, it is occasionally necessary to identify commercial products by manufacturer's name or label. In no instance does such identification imply endorsement by the National Institute of Standards and Technology, nor does it imply that the particular product or equipment is necessarily the best available for the purpose.

[6]   Although the inlet spherical volume is not part of the SMSS we include it as part of the numerical domain because the velocity and pressure are both known along the surface of the spherical inlet volume, but are not known at the inlet plane of fiber glass bell.

cells by setting the stream-wise velocity gradient to zero. The turbulence intensity is taken to be 5 % at the inlet and outlet planes. We calculated results for pressure drops of ΔP = 1000 Pa and ΔP = 2000 Pa, respectively. The pressure drop of ΔP = 1000 Pa corresponds to an axial flow velocity of W_{avg} = 16.8 m/s in the test section while ΔP = 2000 Pa corresponds to W_{avg} = 25.54 m/s.[7]

The RANS equations are discretized using the finite-volume method with cell-centered vertices. We used an unstructured mesh consisting of 9.8×10^6 cells. The mesh was refined near the pipe walls to capture the turbulent boundary layer. We implemented a first order upwind numerical algorithm which converged in 3000 iterations. The largest residual is the turbulent kinetic energy which is 2×10^{-3}.

Figure 8 shows the normalized axial velocity (u/U_{avg}) in the reference section plotted versus the transverse directions y and z for a specified pressure drop ΔP = 1000 Pa. Here, the average velocity in the reference section is U_{avg} = 30.2 m/s. Plots of the velocity profile are shown at three distances downstream from the fiber glass cone including, x = 0, x = 8 D_{ref}, and x = 15 D_{ref}. As expected, the velocity profile leaving the fiber glass cone at x = 0 is nearly flat. As the flow develops in the reference section viscous effects retard the velocity near the wall resulting in increased velocities in the core flow at x = 8 D_{ref} and x = 15 D_{ref}. Moreover, the calculations showed that the non-axial velocity components at x = 15 D_{ref} are nearly zero. The velocity field is axisymmetric and nearly swirl-free at the location where the USM will be installed to measure flow (*i.e.*, x = 17.4 D_{ref}). Based on these results installation effects will not influence the flow measurement in the reference section.[8]

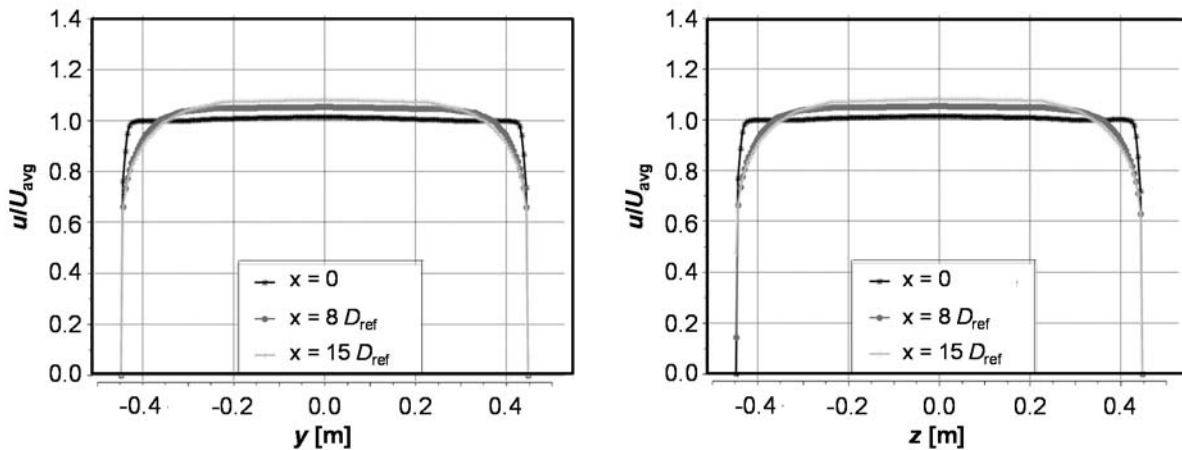**Figure 8.** Plot of normalized axial velocity in the reference section (u/U_{avg}) versus y and z at axial locations x = 0, x = 8 D_{ref} and x = 15 D_{ref} for a specified pressure drop of 1000 Pa (*i.e.*, U_{avg} = 30.2 m/s).

Calibration of the USM in the Reference Section
The 8 path ultrasonic flow meter (USM) was calibrated in a blow-down facility against an array of 8 critical flow venturis (CFVs) [20]. Each of the CFVs had a nominal throat diameter of 2.54 cm

---

[7]   Following conventional fluid mechanics notation the velocities in the x, y, and z directions are u, v, and w, respectively. Similarly, the average velocities in the reference section and test section shown in Fig. 7 are U and W respectively.

[8]   Here we assume that the flow entering the intake module is swirl-free.

and was traceable to NIST's primary flow standards. Figure 9 shows the USM installed in the blow-down facility. The entire reference section shown in Fig. 6 as well as the fiber glass cone shown in Fig. 4C were installed in the blow down facility and calibrated together with the USM in the same configuration as used in the SMSS.[9]
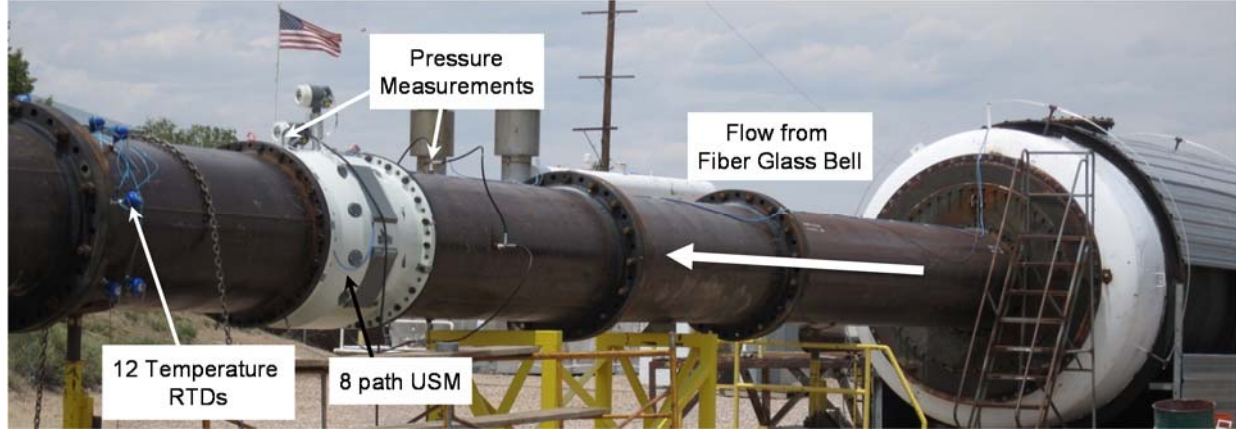

Figure 9. Installation of SMSS reference pipe section including USM installed in blow-down facility for calibration.

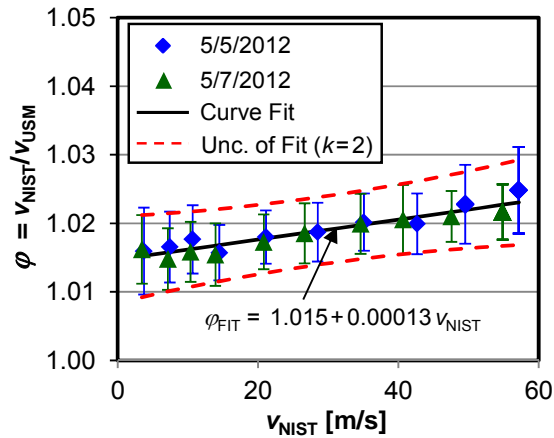$$\varphi_{FIT} = 1.015 + 0.00013\, v_{NIST}$$

Figure 10. Calibration data of 8 Path USM.

The USM was calibrated at atmospheric pressure in dry air over velocities ranging from 3 m/s to 57 m/s. Figure 10 shows a plot of the calibration results. The calibration factor, $\phi = V_{NIST}/V_{meter}$, is the ratio of the velocity determined by the upstream CFV working standards divided by the USM reported velocity. The conservation of mass (accounting for storage effects in the connecting volume) is used to relate the mass flow at the upstream CFV array ($\dot{m}_{CFVarray}$) to the mass flow at the USM ($\dot{m}_{USM}$). The USM mass flow is converted to velocity by dividing by the density and cross sectional area of the USM, $V_{NIST} = \dot{m}_{USM}/\rho_{USM} A_{USM}$, where ρ_{USM} is the density of dry air at the measured pressure and temperature, and A_{USM} is the cross-sectional area of the USM.

The calibration was performed on two occasions, first on 5/5/2012, and a second time on 5/7/2012. The expanded uncertainty of the calibration factor ranged from 0.45 % to 0.58 % over

---

9   Note that the exterior of the reference piping was painted white after the calibration at the blow-down facility.

the velocities from 3 m/s to 57 m/s. However, over the narrower range of velocities used in the SMSS (10.7 m/s to 46.2 m/s) the expanded uncertainty can be taken to be 0.5 %.
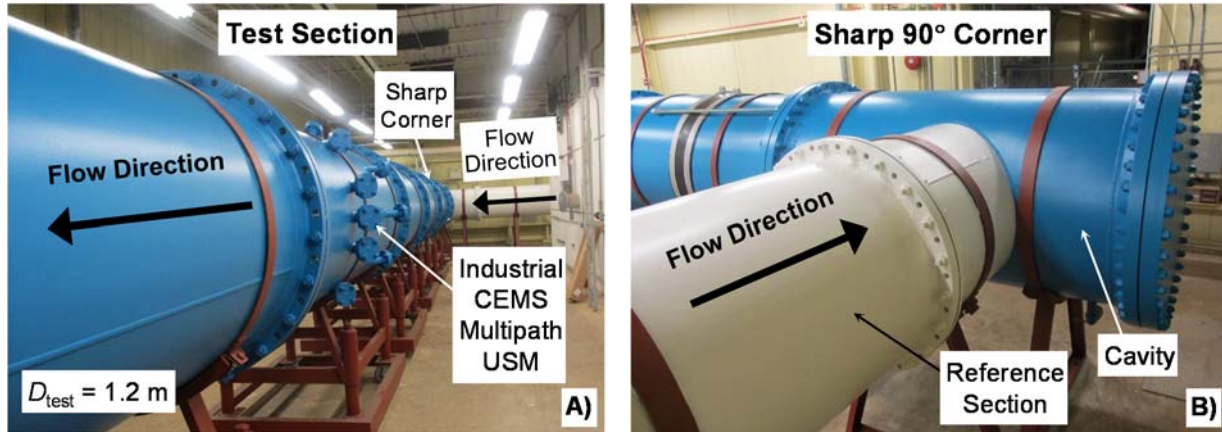

Figure 11. A) Test section of SMSS showing industrial multipath ultrasonic flow meter, and B) Sharp 90° corner between reference section and test section.

3.3. Establishing Smokestack-like Velocity Fields in the Test Section

The SMSS test section is designed to produce the distorted flow conditions typically found in CFPP smokestacks. The flow in the test section consist of a swirling flow with an asymmetric axial velocity profile. The velocity distortions in the SMSS test section are produced using a piping arrangement commonly used in CFPP smokestacks (*i.e.*, the sharp 90° elbow shown in Fig. 2 and in Fig. 11B). The axial velocity (W_{avg}) ranges from 6 m/s to 26 m/s to correspond with the velocity range in CFPP smokestacks. In this way the differential pressure measured during pitot traverses will be comparable to those in CFPP smokestacks.
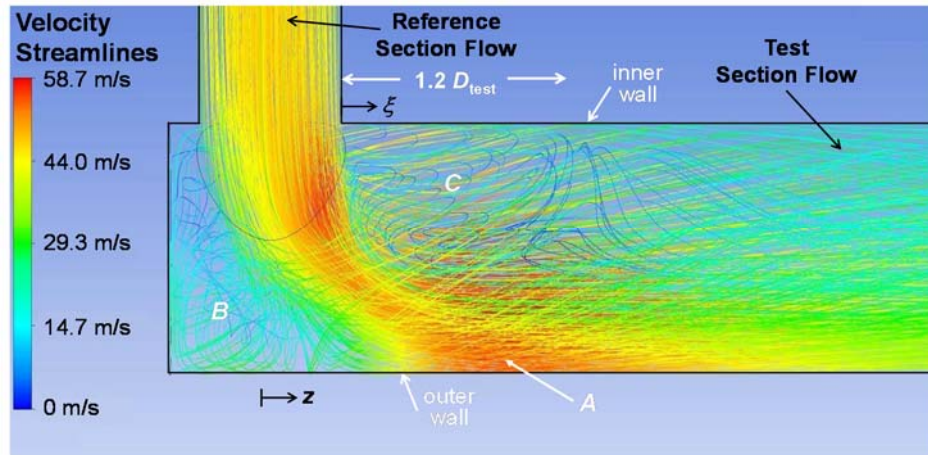

Figure 12. CFD computations of streamlines in the sharp 90° elbow for test section velocity of W_{avg} = 25.5 m/s (*i.e.*, ΔP = 2000 Pa): A) High velocities skewed toward outer wall of sharp 90° elbow, B) Recirculation zone in cavity at the base of the test section, C) Separated flow region on inner wall of sharp 90° elbow.

Figures 11A and 11B show the test section and the sharp 90° elbow responsible for distorting the flow. We computed flow in 90° elbow for a pressure drop of ΔP = 2000 Pa specified at the exit of the SMSS. The computational results are shown in Fig. 12. Streamlines emanating from the

reference section are skewed toward the outer wall of the sharp 90° elbow (A). This region of high velocity is more than twice the average flow velocity W_{avg} = 25.5 m/s. As expected the CFD model predicts a recirculation in the cavity at base of the test section (B). A second recirculation zone forms in the test section along the inner wall of the sharp 90° elbow (C). The separated flow region extends along the inner wall of the elbow beginning at ξ = 0 and extends to the reattachment point located at ξ = 1.2 D_{test} as shown in the figure. For a pressure drop of ΔP = 1000 Pa the reattachment point is slightly shorter, ξ = 1.1 D_{test}. However, in general the results for ΔP = 1000 Pa are similar to the results for ΔP = 2000 Pa.

Computed Velocity Field in the Test Section

Figure 13A and 13B show the normalized axial velocity (w/W_{avg}) for a pressure drop ΔP = 1000 Pa plotted against the transverse directions x_{test} and y, respectively.[10] Four axial velocity profiles are shown corresponding to ξ = 0, ξ = 4 D_{test}, ξ = 8 D_{test}, and ξ = 12 D_{test} where the parameter ξ = z - D_{ref}/2 measures the axial distance in the test section relative to the exit plane of the sharp 90° elbow. In this way ξ specifies the length of constant diameter piping downstream from the structure causing the installation effect. At ξ = 0, Fig. 13A shows the normalized axial velocity component, w/W_{avg}, is skewed toward the outer wall of the sharp 90° elbow with reverse flow along the inner wall. Further downstream at ξ = 4 D_{test}, significant profile effects remain. Although the boundary layer has reattached, w/W_{avg} remains significantly skewed. At ξ = 8 D_{test} and ξ = 12 D_{test} the skew remains but is significantly less.
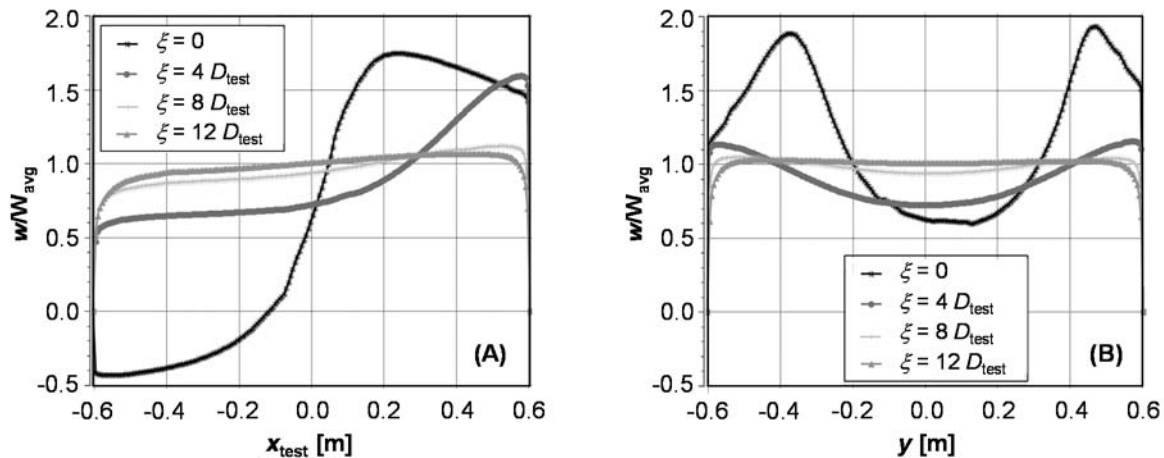

Figure 13. Plots of the normalized axial (w/W_{avg}) and transverse (u/W_{avg} and v/W_{avg}) velocity components in the test section of the SMSS versus transverse directions x_{test} and y. (Computations correspond to ΔP = 1000 Pa and plots are made at four downstream distances from the exit plane of the sharp 90° elbow; ξ = 0, ξ = 4 D_{test}, ξ = 8 D_{test}, and ξ = 12 D_{test}.)

Along the y-axis Fig. 13B shows pronounced wall jetting at the exit plane of the elbow (*i.e.,* ξ = 0). Axial velocities near the wall reach speeds nearly 2 times W_{avg}. In contrast, near y = 0 the speed slows to nearly 0.5 W_{avg}. Further downstream at ξ = 4 D_{test} viscous effects have significantly

---

[10] For convenience, x_{test} is used instead of x. Here, the origin of the x_{test}-axis is located at y = 0, z = 0.5 D_{test}, and x = 25.5 D_{ref} + 0.5 D_{test} (see Fig. 7). In this way x_{test} is located at the exit plane of the sharp 90° elbow and varies from x_{test} = D_{test}/2 at the outer wall to x_{test} = - D_{test}/2 at the inner wall.

reduced jetting effects, but residuals from the elbow profile remain. At $\xi = 8\ D_{test}$ and $\xi = 12\ D_{test}$ jetting effects are dissipated and the velocity profile is nearly flat.

Initial testing in the SMSS will use the sharp 90° corner to produce the distorted velocity profile and swirling flow in the test section. In later research a perforated plate *flow de-conditioner* will be installed downstream of the sharp corner and used to simulate other common types of installation effects. Herrmann *et. al.* demonstrated that a perforated plate with appropriately sized and angled apertures can be used to produce swirl patterns and velocity profiles that correspond to common piping installations [21].
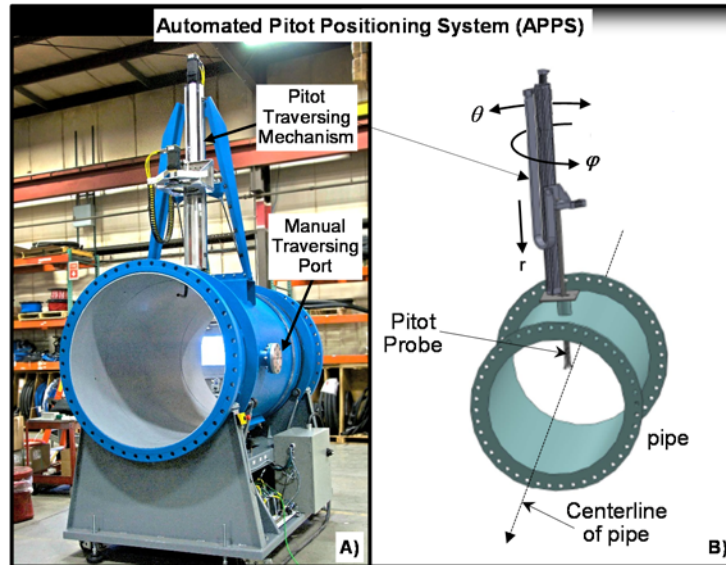

Figure 14. Automated Pitot Positioning System (APPS) including 1 translation stage in the *r*-direction and 2 rotational stages in the φ and θ directions.

Table 1: Range of Motion and Uncertainty of the 3 - axis of APPS

Traversing Axis	Maximum Range of Motion	Expanded Uncertainty
θ	200°	< 1°
φ	360°	< 0.5°
x	1.2 m	< 0.5 mm

3.4. Assessment of EPA Flow RATA in SMSS Test Section

One of the primary functions of the SMSS is to characterize the performance of pitot traversing methods. Figure 1B showed a hypothetical velocity sampling strategy typical of a flow RATA. In this hypothetical example the traverse points (●) were distributed along 2 diametric chords oriented at $\theta_1 = 135°$ and $\theta_2 = 225°$, respectively. Since the velocity profile is skewed (Figs. 13A and 13B), the flow velocity determined by the pitot traverse will vary with the probe installation angle (θ). Other important parameters affecting the accuracy of the pitot traverse include the probe

type, swirl level, length of straight pipe (ξ) downstream of the sharp 90° elbow, number of traverse points, and the integration method.

We designed a 3-axis automated pitot positioning system (APPS) shown in Fig. 14 to assess the sensitivity of these parameters on the flow velocity determined from pitot traverse methods. The APPS has 3 traversing stages including a linear traversing stage in the r-direction, and 2 rotational stages in the φ and θ directions as shown in Fig. 14B. The φ-direction rotates the pitot probe about its axis, and will be used to null the S-type pitot probe. The θ-direction rotates the entire pipe section about the pipe centerline. By rotating the pipe by an appropriate angle θ and then traversing the probe by an appropriate distance in the r-direction, a pitot probe can be positioned at any *user selected* location in the cross section. The range and accuracy of the 3 stages are specified in Table 1. We will vary the traverse parameters to assess a variety of pitot traverse sampling methods (including the EPA RATA). The accuracy of these pitot traverse sampling methods will be quantified using the flow determined by the 8 path USM installed in the reference section.
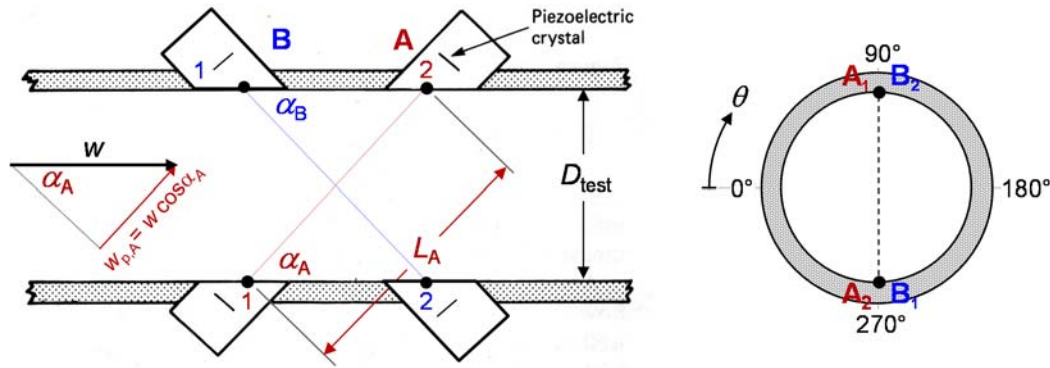

Figure 15. Schematic shows a typical CEMS Ultrasonic flow monitor with 2 symmetrical crossing paths A and B installed into a pipeline of diameter D_{test}.

3.5. Assessment of CEMS Flow Monitor in Test Section

The SMMS facility will be used to characterize CEMS ultrasonic flow monitors. CEMS flow monitors generally have either a single diametric path or two symmetrically crossing paths (*i.e.*, the x-pattern configuration). A sketch of these both configurations is shown in Fig. 15. The single path configuration is displayed by either path A or B by itself, and the *x-pattern* configuration is shown by the 2 paths A and B together. Paths A and B are oriented at path angles of α_A and α_B respectively, and at installation angles of θ_A = 90° and θ_B = 270°. The straight line paths A and B are respectively the trajectories of an ultrasonic sound wave emitted from A_1 to A_2 (*i.e.*, path A) and from B_1 to B_2 (*i.e.*, path B) for zero flow. These paths can be approximated as straight for the low Mach number flows in CFPPs smokestack (*i.e.*, Mach number less than 0.1).

An ultrasonic flow meter measures the transit time of an ultrasonic sound wave to travel a known distance with and against the flow velocity. The transit time for the sound wave to travel with the flow (t_{with}) velocity differs from the travel time against the flow ($t_{against}$) as a function of the velocity along the path. As such, the transient times t_{with} and $t_{against}$ in conjunction with the path length can be used to determine the *average velocity along the path*. For path A in Fig. 15 the

average velocity along the path is $w_{p,A}$. For a uniform and swirl-free flow (*i.e.*, no transverse velocity components) the flow velocity is $w = w_{p,A}/\cos\alpha_A$ where the average path velocity is divided by $\cos\alpha_A$. The analogous expression for path B is $w = w_{p,B}/\cos\alpha_B$.

Since CFPP smokestacks have swirling flow with skewed velocity profiles the ultrasonic flow meters have both 1) velocity profile errors and 2) swirl errors. Moreover, the velocity varies with the installation angle because the path slices through a different section of the velocity profile as θ varies. For the same reason the velocity will also depend on the path angle (α). The errors associated with these effects can be mitigated by using multipath configurations. For example, the *x-pattern* configuration in Fig. 15 reduces errors associated with swirl. Analogously, profile errors can be reduced by multiple coplanar paths. These path configurations have been demonstrated to reduce profile and swirl errors in ultrasonic meter flow measurements [22 - 26].

NIST will use the industrial ultrasonic flow meter installed in the test section shown in Fig. 11A to assess the performance of a single diametric path and the x-pattern path configuration typically used in CEMS flow monitors. We will characterize the performance as a function of installation angle and downstream distance from sharp 90° elbow. Future studies will characterize the performance of multipath configurations.

SUMMARY AND CONCLUSIONS

NIST built a scale-model smokestack simulator (SMSS) 1/10th the scale of an industrial CFPP smokestack. The test section of the SMSS will have the same velocity range and similar flow distortions found in a typical CFPP smokestack. However, the SMSS will provide reference flow measurements at expanded uncertainties of less than 1 %, in contrast to CFFP which are estimated to have errors in excess of 10 %. The documented flow traceability of the SMSS will enable NIST to determine the flow component of uncertainty of pitot traversing methods used in the EPA flow RATA, and CEMS flow monitors installed in CFFP smokestacks. The facility will be used to research new methods for improved flow measurement, and to provide benchmark data to validating CFD calculations, which will be used to scale-up SMSS results to industrial scale CFPPs. Finally, the SMSS facility can be used for proficiency testing of RATA companies who routinely perform EPA pitot traverses to calibrate the CEMS flow meters used in CFPPs.

REFERENCES

[1]   Tarr J. M., and Adair, S., ***The EPA's Proposed Guidelines for Regulating Carbon Dioxide Emissions from Existing Power Plants***, Nicholas Institute for Environmental Policy Solutions, Duke University, June 2014.

[2]   Borthwick, R., Whetstone, J., Yang, J. C., and Possolo, A., ***Examination of United States Carbon Dioxide Emission Databases***, EPRI CEM User Group Conference and Exhibit, Chicago, IL., June 2011.

[3]   Quick, J. C., ***Carbon Dioxide Emission Tallies for 210 U.S. Coal-fired Power Plants: A Comparison of Two Accounting Methods***, Journal of the Air & Waste Management Association, Volume 64, Issue 1, Pg. 73 – 79, Dec. 2013.

[4]   Traina, J. E., ***Reduce Flow Bias through Automated Testing***, The 20th Annual Electric Utility Chemistry Workshop, Champaign, Illinois, May 2000.

[5]   Trang, N. D., Kang, W., Shim J. S., Jang H. S, Park, S. N., and Choi, Y. M., ***Experimental Study of the Factors Effect on the S-Type Pitot Tube Coefficient***, XX IMEKO World Congress Metrology for Green Growth, Busan, Republic of Korea, September 2012.

[6]   Kang, W., Trang, N. D., Shim J. S., Jang H. S, and Choi, Y. M., ***Experimental and Numerical Investigations of Factors Effect on the S-Type Pitot Tube Coefficients***, The 16th International Flow Measurement Conference FLOMEKO 2013, Paris France, September 2013.

[7]   Reader-Harris M., ***Flowrate measurements using Pitot tubes to measure emissions in circular ducts***, International Symposium on Fluid Flow Measurement (ISFFM), Colorado Springs, Colorado, 2012.

[8]   Environmental Protection Agency**, *40 CFR Part 60 Application Method 1 Traverse Points - Stationary Sources***, Washington D.C., 1996.

[9]   Environmental Protection Agency**, *40 CFR Part 60 Application Method 2 Velocity and S-type Pitot*,** Washington D.C., 1996.

[10]   Environmental Protection Agency**, *40 CFR Part 60 Application Method 2C Velocity & Flow Rate - Standard Pitot*,** Washington D.C., 1996.

[11]   Environmental Protection Agency**, *40 CFR Part 60 Application Method 2F Stack Gas-Velocity/Volumetric Flow Rate-3D probe*,** Washington D.C., 1996.

[12]   Environmental Protection Agency, ***40 CFR Part 60 Application Method 2G Stack Gas-Velocity/Volumetric Flow Rate-2D probe***, Washington D.C., 1996.

[13]   Environmental Protection Agency, ***40 CFR Part 60 Application Method 2H* Stack Gas Velocity / (Decay Near Stack Wall)**, Washington D.C., 1996.

[14]   Norfleet, S. K., Muzio L. J., and Martz T. D., ***An Examination of Bias in Method 2 Measurements Under Controlled Non-Axial Flow Conditions***, Report by RMB Consulting and Research, Inc.

[15]   Crowley, C. J., Shinder, I. I., Moldover, M. R., ***The Effect of Turbulence on a Multi-Hole Pitot Calibration***, Flow Measurement and Instrumentation, Vol. 33, pp. 106-109, June 2013.

[16]   Norfleet, S. K., and Roberson, W. R., ***Part 75 CEMS Equipment - What's Everyone Using? A Look at Current Trends in CEMS Providers***, EPRI CEMS Users Group Meeting, San Diego, CA, May 2003.

[17]   Verkaik A., C., ***Analysis of Velocity Profiles in Curved Tubes,*** Eindhoven University of Technology, Feb. 2008.

[18]   Mossad, R., Yang, W., Schwarz,. M. P., ***Numerical Prediction of Air Flow in a Sharp 90º Elbow***, Seventh International Conference on CFD in the Minerals and Process Industries CSIRO, Melbourne, Australia, Dec. 2009.

[19]   Mattingly, G. E., and Yeh T. T., ***NBS' Industry Government Consortium Research Program on Flow meter Installation Effects; Research Period January – July 1988,*** NIISTIR 89-4080, April 1989.

[20]   Johnson, A. N., Harman, E., Boyd, J. T., ***Blow-Down Calibration of a Large 8 Path Ultrasonic Flow Meter under Quasi-Steady Flow Conditions***, The 16th International Flow Measurement Conference FLOMEKO 2013, Paris France, September 2013.

[21]   Herrmann, V., Dietz, T., and Wehmeier, M., ***Reliability and Installation Effects of Ultrasonic Custody Transfer Gas Flow Meters Under Special Conditions,*** 4th International South East Asia Hydrocarbon Flow Measurement Workshop, March 2005.

[22]   Zhang, L., Hu, H., Meng, T., & Wang, C. ***Effect of Flow Disturbance on Multi-Path Ultrasonic Flowmeters***, IMEKO TC9, 2013.

[23] Hackett, D., *Fundamentals of Multipath Ultrasonic flow meters for Gas Measurement*, American School of Gas Measurement Technology Organization: American School of Gas Measurement Technology, 2012.

[24] Lansing, J., *Multipath USMs for Gas Measurement*, International School of Hydrocarbon Measurement (ISHM), 2008.

[25] Grimley, T. A. *Multipath Ultrasonic Flowmeter Performance*., Proceedings of AGA Operating Section, pp. 566-570., 1996.

[26] Vulovic, F., Harbrink, B., and Bloemendaal. K. van, *Installation effects on a multipath ultrasonic flow meter designed for profile disturbances*, North Sea Flow Measurement Workshop, 1995.